Dynamics of Rydberg states and terahertz waves generated in strong few-cycle laser pulses

Jinlei Liu,[1,*] Jing Zhao,[1] Yindong Huang,[1,2] Xiaowei Wang,[1] and Zengxiu Zhao[1,†]
[1]*Department of Physics, National University of Defense Technology, Changsha 410073, People's Republic of China*
[2]*National Innovation Institute of Defense Technology, AMS, Beijing 100071, People's Republic of China*

(Received 15 November 2019; accepted 2 July 2020; published 10 August 2020)

Physical processes near threshold in strong-field ionization are complex owing to the important role of many intermediate states. Two typical near-threshold processes in few-cycle laser pulses, the generations of Rydberg electrons and terahertz waves, are investigated using classical trajectory Monte Carlo simulations. Mapping final energies of electrons to the tunneling coordinates, the two processes are distinguished based on the contributions from different kinds of electron trajectories, which highlights the complex interplay between the Coulomb potential and the laser field on the electron dynamics. We clarify the dependence of momentum and energy spectra on the carrier-envelope phase. We find that the optimal phases for terahertz wave generation and creation of the Rydberg state in few-cycle laser pulses are opposite. This finding can be applied to further experiments on attosecond electron dynamics.

DOI: 10.1103/PhysRevA.102.023109

I. INTRODUCTION

It is difficult to describe the behaviors of physical systems near threshold due to the lack of accurate physical models. For an atom or a molecule exposed to a high-intensity laser pulse, many highly nonlinear strong-field phenomena appear above the ionization threshold such as high harmonic generation, high-above-threshold ionization, and nonsequential double ionization [1–3]. The involved dynamics can be well understood with a three-step model [4] where the strong-field approximation [5–7] serves as an analytical tool to describe the rescattering process. The strong-field approximation is based on a few assumptions such as treating the laser electric field classically and neglecting the ionic potential and the electronic structure after ionization. Recently, investigations of dynamics near the ionization threshold are drawing more attention, like low-energy structure [8,9], frustrated tunneling ionization [10–12], below-threshold high-order-harmonic generation [13,14], and terahertz (THz) wave generation [15,16]. The importance of interplay between the Coulomb potential and the laser field in the dynamics of the electron wave packet is proved in these near-threshold phenomena, showing complex threshold characteristics [17].

Rydberg states created in a strong laser field have been studied for several decades. A multiphoton excitation mechanism is always used to explain the generation of neutral excited atoms [18,19], before frustrated tunneling ionization, as a completion of the tunneling-rescattering scenario, is proposed to add the possibility of direct nonradiative capture into excited states of the neutral atom [10]. The excited electron behaves as a quasifree electron during the pulse duration, so it is reasonable to describe these bound states using trajectories obtained from Newton's equations, although the quantum phase information is neglected [20,21]. Tunneling coordinates of Rydberg states, defined as the laser vector potential and the electron's transverse momentum at the instant when the electron tunnels out [22], are verified as starting before and after the field maximum and small perpendicular momentum [23–28]. Half-cycle pulses in the THz frequency range have been widely used in investigating and controlling Rydberg states because their duration is of the same (or a near) order as the orbiting time of a highly excited Rydberg electron [29]. Recently, a pair of optical half-cycle pulses was also utilized to gain better insight into the roles of Coulomb force and the initial lateral momentum distribution in the generation of Rydberg states [12].

Study of THz wave generation is of great interest due to the increasingly wide variety of applications, such as industrial quality control, airport security and environmental studies, and medical diagnostics and treatment [30,31]. The development of highly bright, efficient THz sources is still a challenge holding back the future development of THz science and technology. As a well-established approach, intense THz radiation from gases ionized in strong laser fields has attracted great interest recently, due to its extremely broad bandwidth, which helps to close the "THz gap" [32]. The broken symmetry of the laser-gas interaction can enhance the field strength of emitted THz waves by several orders of magnitude, either by using two-color pulses [33] or by using a carrier-envelope phase (CEP)–stabilized few-cycle pulse [34]. To explain the enhancement, a transient photocurrent model is proposed considering the subsequent electron dynamics following ionization [35,36], while the effect of the Coulomb potential on the motion of the continuum wave packet cannot be neglected [15,37]. Residual photocurrents play an important role in THz wave generation which is modulated in asymmetrical laser pulses such as two-color pulses and few-cycle pulses [38–41]. In a linearly polarized laser field, photocurrents are mainly contributed by low-energy electrons with an energy smaller than $2U_p$, where U_p is the ponderomotive energy, and

*liujinlei@nudt.edu.cn
†zhaozengxiu@nudt.edu.cn

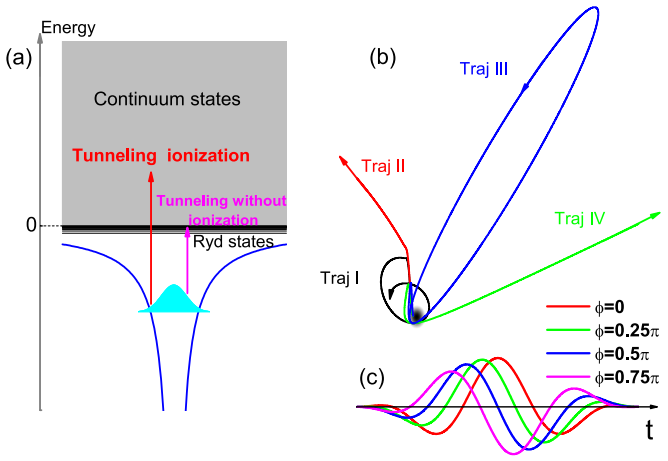

FIG. 1. Schematics of Rydberg states and THz wave generation in the few-cycle laser field. (a) THz emission can be attributed mainly to continuum-continuum transitions after tunneling ionization, while Rydberg states are generated from electrons tunneling out without ionization. (b) Trajectories I, II, III, and IV represent escaping electrons with $E_f < 0$, escaping electrons with $E_f > 0$, rescattering electrons with $E_f < 0$, and rescattering electrons with $E_f > 0$, respectively, where E_f is the electron's final energy. (c) Few-cycle pulses with different CEPs ϕ.

a shift in the photoelectron final energy distribution caused by the Coulomb potential affects the momentum modulations significantly [22]. As in a circularly or elliptically polarized laser field, an offset angle of the residual photocurrent appears which is closely dependent on the laser intensity and atomic structure [42–45]. Recently, THz wave generation was found to be efficiently enhanced by circularly polarized two-color laser fields, compared with linearly polarized two-color laser fields [46,47].

The pulse duration of THz wave is of (or near) the same order as the orbital time of a highly excited Rydberg electron and the classical trajectory method considering the Coulomb potential is well applicable in both Rydberg states and THz wave generation in a strong field [10,15]. However, to the best of our knowledge, there are fewer discussions of the connection between these two near-threshold processes. In the energy space shown in Fig. 1(a), the ionization threshold partitions the whole Hilbert space into continuum states, bound states, and an interim part of Rydberg states. THz emission can be attributed mainly to continuum-continuum transitions after tunneling ionization, while Rydberg states are generated from electrons tunneling out without ionization. Four kinds of trajectories—I, II, III, and IV—shown in Fig. 1(b), represent escaping electrons with $E_f < 0$, escaping electrons with $E_f > 0$, rescattering electrons with $E_f < 0$, and rescattering electrons with $E_f > 0$, respectively, where E_f is the electron's final energy. Although both escaping electrons and rescattering electrons could contribute to Rydberg state and photocurrent generation, the proportion of different kinds of trajectories varies dramatically. For photoelectron yields and the corresponding asymmetry change with the kind of trajectory; electrons which have soft collisions with the atomic core make the main contribution to THz wave generation [15,22,41]. However, electrons released in a narrow time window before the extrema of the oscillating laser field, which experience no rescattering, mainly contribute to Rydberg state generation [23,25]. The change of electric-field's asymmetry in few-cycle pulses with different CEPs, shown in Fig. 1(c), could provide a new perspective on the inherent connection between the two processes, which is meaningful to further quantum control near-threshold phenomena simultaneously in a strong few-cycle field. Note that atomic units (a.u.) are used throughout the paper, unless otherwise stated.

II. METHODS

A. Classical trajectory Monte Carlo (CTMC) simulations

In the calculation, we concentrate on the interaction of the hydrogen atom and the few-cycle laser field. As shown in Fig. 1(c), the laser pulse is chosen to be polarized in the z direction with the form $F(t) = F_0 \sin^2(\omega t/4)\cos(\omega t + \phi)$, where F_0 is the peak electric-field amplitude and $t \in [0, 2T_0]$, with T_0 being the optical period. Electrons are assumed to tunnel out along the polarization axis at every instant t_0 with the initial momentum distribution and ionization rate predicted by the Ammosov, Delone, and Krainov tunneling theory [48,49]. The ionization rate is given by

$$W_0(t_0) = 4\left(\frac{2\kappa^2}{F(t_0)}\right)^{\frac{2}{\kappa}-1} \exp\left[\frac{-2\kappa^3}{3F(t_0)}\right], \tag{1}$$

where $\kappa = \sqrt{2I_p}$, with I_p being the atomic ionization potential. The initial longitudinal momentum (along the instantaneous laser polarization) is 0 and the initial transverse momenta $p^i_\perp$ (perpendicular to the instantaneous laser polarization) are distributed with the probability

$$W_1(p^i_\perp) = \frac{p^i_\perp}{\pi}\frac{\kappa}{F(t_0)} \exp\left[\frac{-\kappa(p^i_\perp)^2}{F(t_0)}\right]. \tag{2}$$

With each electron trajectory weighted by

$$W(t_0, p^i_\perp) = W_0(t_0)W_1(p^i_\perp), \tag{3}$$

more than 1 billion trajectories are launched, while the ionization moment and the initial lateral momentum are sampled as two coordinates of a uniform random variable in the parameter space, $[0, 2T_0]$ and $[-3\sigma_\perp, 3\sigma_\perp]$, where $\sigma_\perp = \sqrt{F(t_0)/\kappa}$ is the width of $p^i_\perp$'s Gaussian distribution. The initial momenta are set as $p^i_x = p^i_\perp \cos(\alpha)$ and $p^i_y = p^i_\perp \sin(\alpha)$, where α is the angle between $p^i_\perp$ and the x axis and is distributed equally within the interval $[0, 2\pi)$ [22,45]. Rewriting the Schrödinger equation in the parabolic coordinates $\xi = r + z$ and $\eta = r - z$, one finds that the effective potential along the η axis at the tunneling moment satisfies

$$V_{\rm eff}(\eta, F(t_0)) = -\frac{1-\sqrt{2I_p}/2}{2\eta} - \frac{1}{8}\eta F(t_0) - \frac{1}{8\eta^2} = -\frac{1}{4}I_p, \tag{4}$$

and the initial tunneling position is determined using $r_0(t_0) = -\frac{\eta}{2}$ along the laser polarization [43,50].

Integrating Newton's equation under the combined field of the laser field and the Coulomb potential, the position $\mathbf{r}$ and the momentum $\mathbf{q}$ of an electron at the end of the laser pulse are obtained, while the angular momentum $\mathbf{M} = \mathbf{r} \times \mathbf{q}$ and the Laplace-Runge-Lenz (LRL) vector $\mathbf{A}_{\rm LRL} = [\mathbf{q} \times \mathbf{M}] - \frac{\mathbf{r}}{r}$ can be identified [51]. From the energy conservation

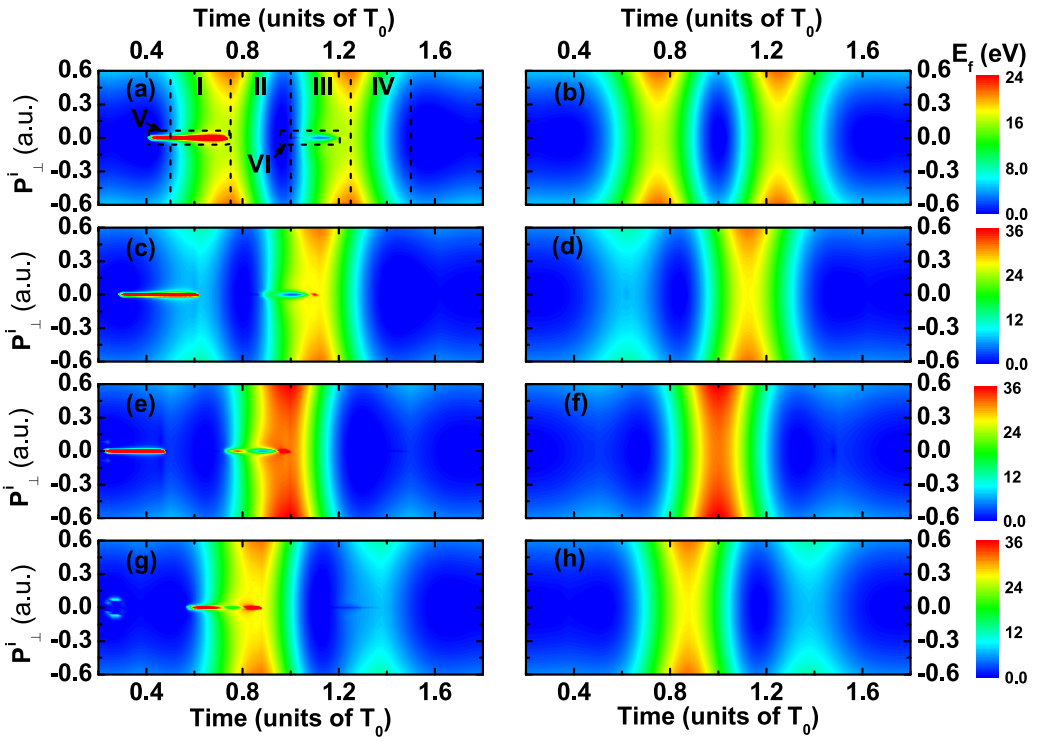

FIG. 2. The calculated photoelectron final energy mapping on the tunneling coordinates (tunneling time and initial transverse momentum $p^i_\perp$). The electrons are under 800-nm laser pulses with a peak intensity of 1.5×10^{14} W/cm^2 and different CEPs ϕ. (a), (b) $\phi = 0$; (c), (d) $\phi = 0.25\pi$; (e), (f) $\phi = 0.5\pi$; (g), (h) $\phi = 0.75\pi$. The two columns represent electrons propagating with and without the Coulomb potential, respectively. Six areas are distinguished by dashed lines and marked according to different kinds of electron trajectories.

law $\frac{p^2}{2} = \frac{q^2}{2} - \frac{1}{r}$, the magnitude of the asymptotic momentum p is determined and the asymptotic momentum $\mathbf{p}$ is calculated using a simple formula [21,52]:

$$\mathbf{p} = p\frac{p(\mathbf{M} \times \mathbf{A}_{\rm LRL}) - \mathbf{A}_{\rm LRL}}{1 + p^2 M^2}. \tag{5}$$

A detailed description of the CTMC method and derivation of Eq. (5) can be found in our previous work [45].

B. Calculation of Rydberg states and photocurrents

To clarify the role of the Coulomb potential in Rydberg state and photocurrent generation, calculations are performed with and without the Coulomb potential. In the latter case, the Coulomb potential is only neglected until the end of the laser pulse, as the Rydberg state definition is dependent on the Coulomb potential. After the laser pulse, the Coulomb force is no longer negligible, capturing electrons into Rydberg states [24]. Using asymptotic momenta obtained from Eq. (5), the total current is calculated by summing over trajectories with final energy $E_f > 0$ using

$$\mathbf{J} = \sum_j W_j(t_0, p^i_\perp)\mathbf{p}_j, \tag{6}$$

while an electron is classified as a Rydberg state if its final energy $E_f < 0$. An effective angular momentum number $l_{\rm eff}$ is determined from

$$|\mathbf{L}^2| = l_{\rm eff}(l_{\rm eff} + 1), \tag{7}$$

where the classical angular momentum $\mathbf{L} = \mathbf{r} \times \mathbf{q}$ [12].

III. RESULTS AND DISCUSSION

In our calculations (see Sec. II for details), two-cycle laser pulses with a wavelength of 800 nm and a peak intensity of 1.5×10^{14} W/cm^2 are chosen, where T_0 is the optical period. For simplicity, our discussion focuses on four CEPs—$\phi = 0,\ 0.25\pi,\ 0.5\pi$, and 0.75π—whose pulses are shown in Fig. 1(c).

A. Energy mapping on the tunneling coordinates (EMTC)

Due to the complex dynamics of electrons in the near-threshold regime, it is very difficult to obtain the specific final state of an electron just according to its initial tunneling information. EMTC makes a bridge between the final state and the initial state of the electron and provides an intuitive picture to further understand the interplay of the Coulomb potential and the laser field. In addition, different kinds of electron trajectories (tunneling without ionization, escaping, forward scattering, and backscattering) can be distinguished using EMTC directly.

As shown in Fig. 2, EMTC of photoelectrons in different CEPs is compared when considering or neglecting the Coulomb potential. In Fig. 2(a), six areas are marked according to different kinds of electron trajectories, with areas I and III representing forward-rescattering electrons, areas II and IV representing escaping electrons, and areas V and VI representing backward-rescattering electrons. In classical analysis, escaping electrons tunnel before the peak of the laser field, while rescattering electrons tunnel mainly after the peak

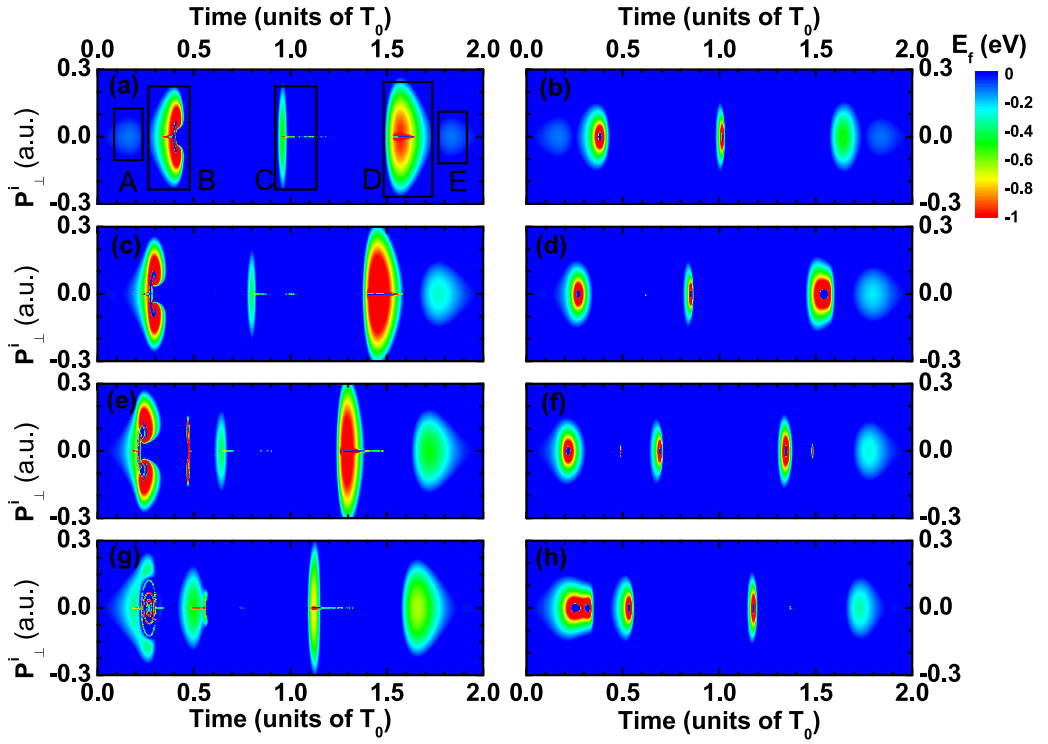

FIG. 3. Rydberg state final energy mapping on the tunneling coordinates with the same laser parameters as in Fig. 2. (a), (b) $\phi = 0$; (c), (d) $\phi = 0.25\pi$; (e), (f) $\phi = 0.5\pi$; (g), (h) $\phi = 0.75\pi$. The two columns represent electrons propagating with and without the Coulomb potential, respectively.

in each half-cycle [2]. In area V, electrons with a small $p_\perp$, i.e., momentum perpendicular to the polarization axis, obtain high energies by being backward rescattered. However, electrons in area VI, which should be the same as in area V, are recaptured in Rydberg states. Under the condition $\phi = 0$, the envelope of the laser field decreases after the main peak at $t = T_0$ and electrons cannot return to the nucleus before the laser pulse finishes and have enough energy to overcome the attraction of the Coulomb potential.

Comparing Figs. 2(a) and 2(b), differences appear in rescattering areas, I, III, V, and VI, where the Coulomb potential cannot be neglected, as electrons return to the nucleus again during their propagation. As shown in Fig. 2(b) when the Coulomb potential is not considered, the final energy of an electron $E_f = \sqrt{A^2(t) + {p^i_\perp}^2}$, where $\mathbf{A}(t)$ and $p^i_\perp$ are the vector potential and the perpendicular momentum at the moment of tunneling. Areas I–IV are exactly the same or symmetric and areas V and VI disappear, as no backscattering occurs without the Coulomb potential. Electrons tunneling slightly before the peak of the laser field could also be rescattered due to the Coulomb focusing effect, transforming the low-energy vacancy from a circular shape into a heart shape between area II and area III and breaking the symmetry of the two areas [22].

When the CEP changes from 0 to 0.75π, the peak of the laser field moves forward and areas I and II disappear and areas III and IV gradually change into I and II, which are the same both considering and not considering the Coulomb potential. High-energy parts appear on both sides of area VI at CEPs of 0.25π, 0.5π, and 0.75π, contributed by backscattering electrons as in area V. The low-energy vacancy between high-energy parts indicates the moment when electrons that tunnel with no perpendicular momentum can return to the nucleus without enough velocity to escape again. Comparing $\phi = 0$ and $\phi = 0.75\pi$, the center of the low-energy vacancy in area VI moves from $1.15T_0$ to $0.9T_0$, with a difference of $0.25T_0$, which is exactly the difference in the peak of the laser field.

In the negative EMTC shown in Fig. 3, Rydberg states are generated in certain windows (A, B, C, D, E), mainly at the leading edge of laser cycles, which is contributed by both direct escape trajectories and rescattering trajectories [23,25]. When the Coulomb potential is ignored, annulus windows appear with a near-zero center, indicating the two paths (long and short) in the rescattering scenario [4]. The windows are much larger and more irregular when the Coulomb potential is considered for chaotic rescattering near the boundary of the windows and a shift of $0.1T_0$ appears for the break of symmetry caused by the Coulomb focusing effect. As discussed above, whether rescattering exists depends on the relative size of the neighboring laser peaks, resulting in a large difference in the shape of windows in the leading vs the trailing edges of the envelope. Accompanying the movement of these windows, the contribution of different kinds of trajectories also changes with the CEP, making a spectral modulation which is discussed in the following.

Similar EMTC changes of photoelectrons and Rydberg states with the CEP have an implication for the synchronization of Rydberg states and THz wave generation. Areas of photoelectrons and windows of Rydberg states are both

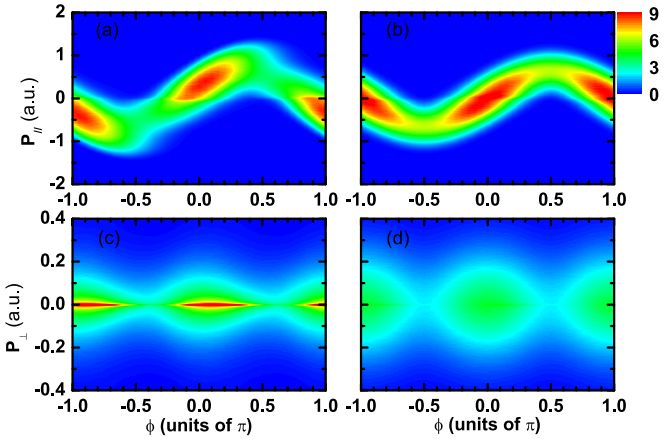

FIG. 4. Comparison of photoelectron momentum spectra under different CEPs ϕ. (a), (b) Momentum parallel to the polarization axis $p_{\parallel}$ and (c), (d) momentum perpendicular to the polarization axis $p_{\parallel}$, with the two columns representing electrons propagating with and without the Coulomb potential, respectively.

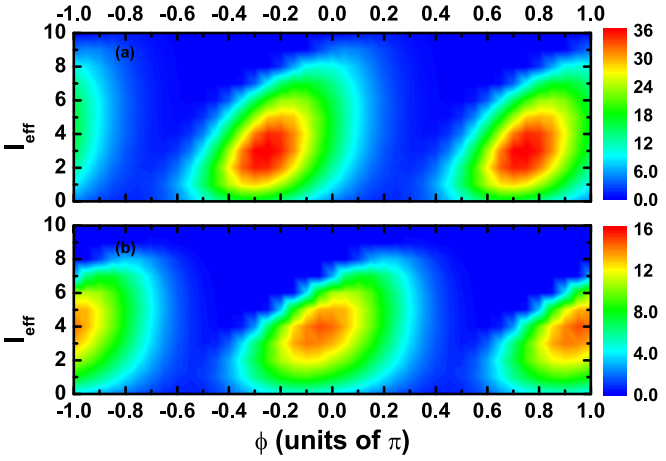

FIG. 5. Comparison of the angular momentum spectra of Rydberg states under different ϕ values (a) with and (b) without consideration of the Coulomb potential, respectively. The effective angular quantum number l_{eff} is calculated from the final angular momentum $\mathbf{L}$ using Eq. (7).

dependent on the side of the envelope (rising or falling) and the Coulomb potential, suggesting the great influence of the rescattering process. Positive and negative EMTCs are complementary to each other, providing an illustrative picture of strong-field ionization.

B. The modulation of spectra: Momentum, angular momentum, and energy

As a fundamental observable in experiments, electrons' spectra, modulating with CEPs of few-cycle laser pulses, provide information on the inherent dynamics. Figures 4(a) and 4(b) and Figs. 4(c) and 4(d) show the calculated photoelectron spectra of the momenta parallel and perpendicular to the polarization axis, $p_{\parallel}$ and $p_{\perp}$, respectively. When the Coulomb potential is neglected, in Fig. 4(b), the center of parallel-momentum spectra exhibits $\sin\phi$ behavior the same as that of the potential vector $\mathbf{A}$. In Fig. 4(d), the momentum perpendicular to the polarization axis $p_{\perp} = p^{i}_{\perp}$, which is correlated positively with the electric-field maximum as in Eq. (2). While the Coulomb potential is considered in Fig. 4(a), the peak of the parallel momentum $p_{\parallel}$ is 0.5 a.u. for the CEP $\phi \in [-0.5\pi, 0.5\pi]$ and -0.5 a.u. for the CEP $\phi \in [-\pi, -0.5\pi] \cup [0.5\pi, \pi]$. A double-hump structure, rather than a peak at $p_{\parallel} = 0$, will be formed as a consequence of rescattering if a multicycle pulse is used [53,54]. In the case of a few-cycle pulse, only one hump appears at a certain CEP, as the rescattering happens only on one side. For the momentum perpendicular to the polarization axis $p_{\perp}$ in Fig. 4(c), the distribution is much more centered and a sharp peak appears due to the Coulomb focusing effect [22].

Angular momentum spectra of Rydberg states with and without consideration of the Coulomb potential are shown in Figs. 5(a) and 5(b), respectively. Rydberg states are mainly generated at the CEP $\phi \in [-0.4\pi, 0.3\pi]$ and the maximum angular momentum $l_{\text{eff}} = 8$ is obtained at $\phi = 0.2\pi$ when the Coulomb potential is neglected in Fig. 5(b). However, when the Coulomb potential is considered in Fig. 5(a), a shift of -0.2π in the spectra appears, which results from the $-0.1T_0$ shift in the negative EMTC results shown in Fig. 3. In addition, the yield of Rydberg states more than doubles when the Coulomb potential is considered, as the window in the negative EMTC is much wider in the lateral direction due to the Coulomb focusing effect [12].

Energy spectra including above-threshold photoelectrons and below-threshold Rydberg states are illustrated in Fig. 6. The optimal phases are determined when the yield attains its maximum in each energy bin, indicated by filled black circles. Optimal phases in negative-energy spectra and positive-energy spectra match well under both conditions: Considering [Figs. 6(a) and 6(c)] and not considering [Figs. 6(b) and 6(d)] the Coulomb potential. When the Coulomb potential is not considered as in Figs. 6(b) and 6(d), a symmetry jump from $\phi = 0$ to $\phi = 0.5\pi$ and to $\phi = -0.5\pi$ occurs when the electron energy $E \approx 0.5U_p$. This is the same as the phase dependence in a two-color laser field and shows the contribution

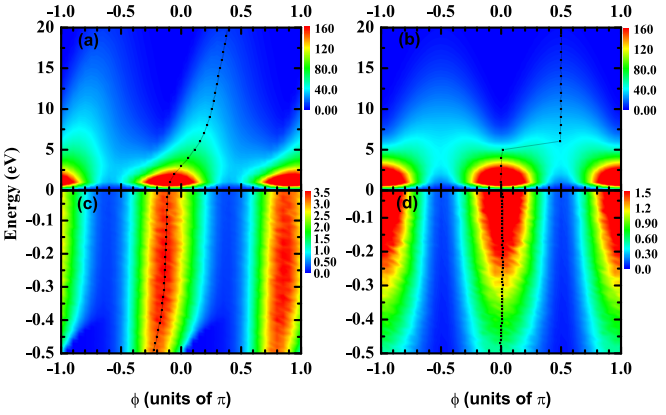

FIG. 6. Energy spectra, including (a), (b) positive energy and (c), (d) negative energy, modulated against the CEP ϕ, with the two columns representing electrons propagating with and without the Coulomb potential, respectively. The optimal phases, at which the yields attain their maximum values in the energy bins, are indicated by filled black circles.

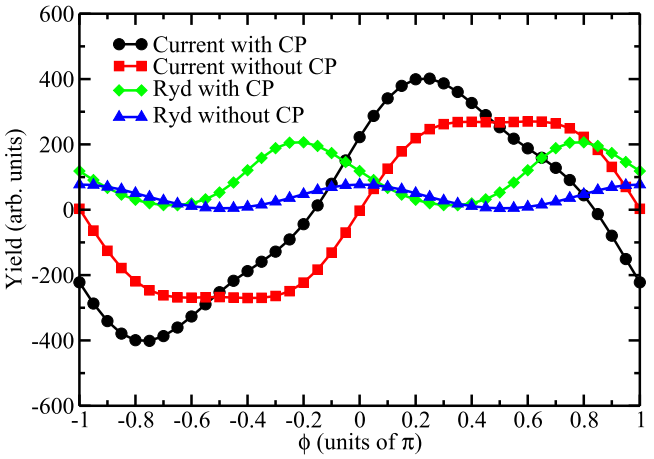

FIG. 7. Comparison of Rydberg states and photocurrent yields as a function of the CEP ϕ. Black circles, red squares, green diamonds, and blue triangles represent photocurrents with the Coulomb potential (CP), photocurrents without the Coulomb potential, Rydberg states without the Coulomb potential, and Rydberg states with the Coulomb potential, respectively.

of both rescattering and escaping electrons [22]. When the Coulomb potential is considered as in Figs. 6(a) and 6(c), the optimal phases indicated by filled black circles are delayed with the increasing energy. With the breaking of the symmetry distribution due to the difference in the contributions of rescattering vs escaping trajectories, the variation of the contribution with the CEP causes a move of the optimal phase from $\phi = -0.2\pi$ to $\phi = 0.7\pi$ with the increasing energy. It should be noted that the negative-energy range discussed is much narrower than the positive-energy range, resulting in a sudden change in the phase gradient near 0.

As shown in Fig. 7, modulations of photocurrents and Rydberg states have almost-opposite optimal phases. When the Coulomb potential is neglected, the Rydberg state generation has an optimal phase of 0 and a plateau centering at 0.5π appears in photocurrent modulation. When the Coulomb potential is considered, the photocurrent attains its maximum at the CEP of 0.25π, and the Rydberg state generation at the CEP of -0.2π. As discussed above, the phase shift of -0.2π in Rydberg state generation corresponds to a move of $-0.1T_0$ in windows of a negative EMTC. For the photocurrents, a phase shift of -0.25π results from the suppression of the path from $\phi = 0$ to $\phi = -0.5\pi$ compared with the path from $\phi = 0$ to $\phi = 0.5\pi$, where forward rescattering plays a vital role due to Coulomb focusing. In addition, the distributions at $\phi = 0.5\pi$ in Fig. 6(b) and at $\phi = 0.25\pi$ in Fig. 6(a) are between 0 and $2U_p$, agreeing with the conclusion in our previous work [15,22,37] that the generation of THz waves is mainly contributed by forward-rescattering electrons with final energy $E_f < 2U_p$. We note that although the optimal CEPs of the two processes in few-cycle laser pulses are opposing, the incompatibility of the two processes in the other laser pulses should be discussed case by case.

IV. CONCLUSION

A complete physical picture of strong-field ionization is developed including the generations of THz waves and Rydberg states. A shift of areas in positive-energy and windows in negative-energy mapping of the tunneling coordinates suggests similar and important roles of the Coulomb potential in the two processes driven by few-cycle pulses. Spectra of the momentum, angular momentum, and energy are modulated with the CEP, showing a variation of contributions from rescattering and escaping trajectories. For the two near-threshold processes, the correlated modulations and similar time scales are analyzed to decode the Coulomb focusing effect on the electronic dynamics. The connection between Rydberg states and THz waves makes it possible to measure their yields simultaneously. Opposing optimal phases of yields in the two processes are obtained, providing the opportunity to realize their simultaneous measurement in experiments.

ACKNOWLEDGMENTS

This work was supported by the National Basic Research Program of China under Grant No. 2019YFA0307703, the Major Research plan of the National Natural Science Foundation of China (Grant No. 91850201), the Natural Science Foundation of China (Grants No. 118074066, No. 11904400, and No.11974426), and the Foundation of National Innovation Institute of Defense Technology (Grant No. XM2019CX5003).

[1] M. Protopapas, C. H. Keitel, and P. L. Knight, Rep. Prog. Phys. **60**, 389 (1997).
[2] F. Krausz and M. Ivanov, Rev. Mod. Phys. **81**, 163 (2009).
[3] W. Becker, X. J. Liu, P. J. Ho, and J. H. Eberly, Rev. Mod. Phys. **84**, 1011 (2012).
[4] P. B. Corkum, Phys. Rev. Lett. **71**, 1994 (1993).
[5] L. V. Keldysh, Sov. Phys. JETP **20**, 1307 (1965).
[6] F. H. M. Faisal, J. Phys. B: At. Mol. Phys. **6**, L89 (1973).
[7] H. R. Reiss, Phys. Rev. A **22**, 1786 (1980).
[8] C. I. Blaga, F. Catoire, P. Colosimo, G. G. Paulus, H. G. Muller, P. Agostini, and L. F. DiMauro, Nat. Phys. **5**, 335 (2009).
[9] W. Quan, Z. Lin, M. Wu, H. Kang, H. Liu, X. Liu, J. Chen, J. Liu, X. T. He, S. G. Chen, H. Xiong, L. Guo, H. Xu, Y. Fu, Y. Cheng, and Z. Z. Xu, Phys. Rev. Lett. **103**, 093001 (2009).
[10] T. Nubbemeyer, K. Gorling, A. Saenz, U. Eichmann, and W. Sandner, Phys. Rev. Lett. **101**, 233001 (2008).
[11] J. Wu, A. Vredenborg, B. Ulrich, L. P. H. Schmidt, M. Meckel, S. Voss, H. Sann, H. Kim, T. Jahnke, and R. Dörner, Phys. Rev. Lett. **107**, 043003 (2011).
[12] B. Zhang, W. Chen, and Z. Zhao, Phys. Rev. A **90**, 023409 (2014).
[13] D. C. Yost, T. R. Schibli, J. Ye, J. L. Tate, J. Hostetter, M. B. Gaarde, and K. J. Schafer, Nat. Phys. **5**, 815 (2009).
[14] M. Chini, X. Wang, Y. Cheng, H. Wang, Y. Wu, E. Cunningham, P.-C. Li, J. Heslar, D. A. Telnov, S.-I. Chu, and Z. Chang, Nat. Photon. **8**, 437 (2014).
[15] D. Zhang, Z. Lü, C. Meng, X. Du, Z. Zhou, Z. Zhao, and J. Yuan, Phys. Rev. Lett. **109**, 243002 (2012).

[16] Y. Huang, C. Meng, X. Wang, Z. Lü, D. Zhang, W. Chen, J. Zhao, J. Yuan, and Z. Zhao, Phys. Rev. Lett. **115**, 123002 (2015).

[17] M. V. Frolov, N. L. Manakov, and A. F. Starace, Phys. Rev. Lett. **100**, 173001 (2008).

[18] M. P. de Boer and H. G. Muller, Phys. Rev. Lett. **68**, 2747 (1992).

[19] E. Wells, I. Ben-Itzhak, and R. R. Jones, Phys. Rev. Lett. **93**, 023001 (2004).

[20] U. Eichmann, T. Nubbemeyer, H. Rottke, and W. Sandner, Nature (London) **461**, 1261 (2009).

[21] N. I. Shvetsov-Shilovski, S. P. Goreslavski, S. V. Popruzhenko, and W. Becker, Laser Phys. **19**, 1550 (2009).

[22] J. Liu, W. Chen, B. Zhang, J. Zhao, J. Wu, J. Yuan, and Z. Zhao, Phys. Rev. A **90**, 063420 (2014).

[23] H. Liu, Y. Liu, L. Fu, G. Xin, D. Ye, J. Liu, X. T. He, Y. Yang, X. Liu, Y. Deng, C. Wu, and Q. Gong, Phys. Rev. Lett. **109**, 093001 (2012).

[24] A. S. Landsman, A. N. Pfeiffer, C. Hofmann, M. Smolarski, C. Cirelli, and U. Keller, New J. Phys. **15**, 013001 (2013).

[25] S. Eilzer and U. Eichmann, J. Phys. B: At. Mol. Opt. Phys. **47**, 204014 (2014).

[26] H. Zimmermann, S. Patchkovskii, M. Ivanov, and U. Eichmann, Phys. Rev. Lett. **118**, 013003 (2017).

[27] S. V. Popruzhenko, J. Phys. B At. Mol. Opt. Phys. **51**, 014002 (2018).

[28] R. Glover, D. Chetty, B. deHarak, A. Palmer, M. Dakka, J. Holdsworth, I. Litvinyuk, A. Luiten, P. Light, and R. Sang, *Frontiers in Optics / Laser Science* (The Optical Society, Washington, DC, 2018), p. JW3A.54.

[29] A. Wetzels, A. Gürtler, L. D. Noordam, F. Robicheaux, C. Dinu, H. G. Muller, M. J. J. Vrakking, and W. J. van der Zande, Phys. Rev. Lett. **89**, 273003 (2002).

[30] M. Tonouchi, Nat. Photon. **1**, 97 (2007).

[31] X. C. Zhang, A. Shkurinov, and Y. Zhang, Nat. Photon. **11**, 16 (2017).

[32] B. Clough, J. Dai, and X. C. Zhang, Mater. Today **15**, 50 (2012).

[33] D. J. Cook and R. M. Hochstrasser, Opt. Lett. **25**, 1210 (2000).

[34] M. Kreß, T. Löffler, M. D. Thomson, R. Dörner, H. Gimpel, K. Zrost, T. Ergler, R. Moshammer, U. Morgner, J. Ullrich, and H. G. Roskos, Nat. Phys. **2**, 327 (2006).

[35] K.-Y. Kim, J. H. Glownia, A. J. Taylor, and G. Rodriguez, Opt. Express **15**, 4577 (2007).

[36] K. Y. Kim, A. J. Taylor, J. H. Glownia, and G. Rodriguez, Nat. Photon. **2**, 605 (2008).

[37] Z. Lü, D. Zhang, C. Meng, X. Du, Z. Zhou, Y. Huang, Z. Zhao, and J. Yuan, J. Phys. B: At. Mol. Opt. Phys. **46**, 155602 (2013).

[38] A. A. Silaev and N. V. Vvedenskii, Phys. Rev. Lett. **102**, 115005 (2009).

[39] W. Chen, Y. Huang, C. Meng, J. Liu, Z. Zhou, D. Zhang, J. Yuan, and Z. Zhao, Phys. Rev. A **92**, 033410 (2015).

[40] V. A. Kostin, I. D. Laryushin, A. A. Silaev, and N. V. Vvedenskii, Phys. Rev. Lett. **117**, 035003 (2016).

[41] Z. Zhou, X. Wang, and C. D. Lin, Phys. Rev. A **95**, 033418 (2017).

[42] P. Eckle, A. N. Pfeiffer, C. Cirelli, A. Staudte, R. Dörner, H. G. Muller, M. Büttiker, and U. Keller, Science **322**, 1525 (2008).

[43] A. N. Pfeiffer, C. Cirelli, M. Smolarski, D. Dimitrovski, M. Abu-samha, L. B. Madsen, and U. Keller, Nat. Phys. **8**, 76 (2012).

[44] L. Torlina, F. Morales, J. Kaushal, I. Ivanov, A. Kheifets, A. Zielinski, A. Scrinzi, H. G. Muller, S. Sukiasyan, M. Ivanov, and O. Smirnova, Nat. Phys. **11**, 503 (2015).

[45] J. Liu, Y. Fu, W. Chen, Z. Lü, J. Zhao, J. Yuan, and Z. Zhao, J. Phys. B: At. Mol. Opt. Phys. **50**, 055602 (2017).

[46] C. Meng, W. Chen, X. Wang, Z. Lü, Y. Huang, J. Liu, D. Zhang, Z. Zhao, and J. Yuan, Appl. Phys. Lett. **109**, 131105 (2016).

[47] V. A. Tulsky, M. Baghery, U. Saalmann, and S. V. Popruzhenko, Phys. Rev. A **98**, 053415 (2018).

[48] M. V. Ammosov, N. B. Delone, and V. P. Krainov, Sov. Phys. JETP **64**, 1191 (1986).

[49] N. B. Delone and V. P. Krainov, J. Opt. Soc. Am. B **8**, 1207 (1991).

[50] L. D. Landau and E. M. Lifshitz, *Quantum Mechanics (Non-relativistic Theory)* (Pergamon, Singapore, 1977), pp. 293–294.

[51] H. Goldstein, C. Poole, and J. Safko, *Classical Mechanics*, 3rd ed. (Addison Wesley, New York, 2000), p. 102.

[52] N. I. Shvetsov-Shilovski, D. Dimitrovski, and L. B. Madsen, Phys. Rev. A **85**, 023428 (2012).

[53] J. Chen and C. H. Nam, Phys. Rev. A **66**, 053415 (2002).

[54] R. Moshammer, J. Ullrich, B. Feuerstein, D. Fischer, A. Dorn, C. D. Schröter, J. R. Crespo Lopez-Urrutia, C. Hoehr, H. Rottke, C. Trump, M. Wittmann, G. Korn, and W. Sandner, Phys. Rev. Lett. **91**, 113002 (2003).